

On the Interaction of Galactic Cosmic Rays with Heliospheric Shocks during Forbush Decreases

Anamarija Kirin¹ · Bojan Vršnak² ·
Mateja Dumbović² · Bernd Heber³

© Springer

Abstract Forbush decreases (FDs) are depletions in the galactic cosmic ray (GCR) count rate that last typically for about a week and can be caused by coronal mass ejections (CMEs) or corotating interacting regions (CIRs). Fast CMEs that drive shocks cause large FDs that often show a two-step decrease where the first step is attributed to the shock/sheath region, while the second step is attributed to the closed magnetic structure. Since the difference in size of shock and sheath region is significant, and since there are observed effects that can be related to shocks and not necessarily to the sheath region we expect that the physical mechanisms governing the interaction with GCRs in these two regions are different. We therefore aim to analyse interaction of GCRs with heliospheric shocks only. We approximate the shock by a structure where the magnetic field linearly changes with position within this structure. We assume protons of different energy, different pitch angle and different incoming direction. We also vary the shock parameters such as the magnetic field strength and orientation, as well as the shock thickness. The results demonstrate that protons with higher energies are less likely to be reflected. Also, thicker shocks and shocks with stronger field reflect protons more efficiently.

Keywords: Cosmic Rays, Galactic; Magnetic fields, Models; Waves, Magneto-hydrodynamic, Shock; Coronal Mass Ejections

✉ A. Kirin
akirin@vuka.hr

✉ B. Vršnak
bvrsnak@geof.hr

¹ Karlovac University of Applied Sciences, Trg J.J.Strossmayera 9, 47000 Karlovac, Croatia

² Hvar Observatory, Faculty of Geodesy, University of Zagreb, Kačićeva 26,10000 Zagreb, Croatia

³ Institut für Experimentelle und Angewandte Physik, Christian-Albrechts-Universität zu Kiel, Christian-Albrechts-Platz 4, 24118 Kiel, Germany

1. Introduction

Forbush decreases (FDs) are depletions in the galactic cosmic ray (GCR) count rate that last typically for about a week, which were first reported by Forbush (1937) and Hess and Demmelair (1937). There are two basic types of FDs depending on their cause. Corotating interacting regions (CIRs) cause “recurrent decreases” which are lower in amplitude, have a gradual onset and symmetric profile (*e.g.* Richardson, 2004). Events related to interplanetary coronal mass ejections (ICMEs) cause “non-recurrent decreases”, which have a sudden onset and a gradual recovery (*e.g.* Lockwood, 1971; Cane, 2000; Belov, 2009). For a more detailed comparison of characteristics of the CIR- and ICME- related FDs see *e.g.* Dumbović *et al.* (2012), Badruddin and Kumar (2016), Melkumyan *et al.* (2019).

Fast CMEs that drive shocks cause large FDs with amplitudes up to 30 % as measured by mid-latitude ground-based neutron monitors (typically observing ≈ 1 GeV particles) that often show a two-step decrease. Traditionally, these are regarded as textbook examples of FDs, where the first step is attributed to the shock and a turbulent region which follows it, while the second step is attributed to the closed magnetic structure (Cane, 2000). The observations show that statistically both regions contribute roughly equally to the total FD magnitude, indicating that shock-related FDs are largest due to the cumulative effect of the magnetic structure and disturbed medium in front of it (Richardson and Cane, 2011). The modelling efforts so far were mainly focused on modelling FDs as a single physical region, where the depression occurs due to scattering related to strong turbulence in the shock/sheath region (Le Roux and Potgieter, 1991; Wawrzynczak and Alania, 2010) or the effects governed by the shock characteristics (*e.g.*, Parker, 1961; Quenby *et al.*, 2008; Krymsky *et al.*, 2009). It was pointed out by Cane 1993 and Wibberenz *et al.* (1998) that it is important to carefully separate the shock/sheath region from the magnetic ejecta region because they are physically different. Indeed, models related to the magnetic structure do separate these two regions (*e.g.* Cane, Richardson, and Wibberenz, 1995; Munakata *et al.*, 2006; Subramanian *et al.*, 2009; Dumbović *et al.*, 2018). However, in order to fully understand the FD, there are strong indications that the shock itself should be decoupled from the sheath region as well.

The interplanetary shocks at 1 AU are practically a discontinuities with typical size $\approx 10^4$ km (Pinter, 1980), which is much smaller than the gyro-radius of the primary GCR corresponding to the detection by ground-based neutron monitor (1 GeV proton in 10 nT field $\approx 10^6$ km). The sheath region at 1 AU is however much larger in size (typically $\approx 10^7$ km at Earth based on Russell and Mulligan, 2002) and comparable to the gyro-radius of 1 GeV protons. Therefore, we might expect that the physical mechanisms governing the interaction with GCRs in these two regions are different. The two-step FDs observed in neutron monitors very often show a precursory increase, possibly resulting from reflection of particles from the shock or acceleration at the shock, although the latter is not considered likely even for very strong shocks (Cane, 2000). Very strong shocks are often associated with series of pre-decreases and pre-increases in the CR intensity accompanied by the changes in the first harmonic of the anisotropy

at the ecliptic plane appearing hours before the FD onset (see *e.g.* Belov *et al.*, 1995, Papailiou *et al.*, 2012, Lingri *et al.*, 2019, and references therein). From that perspective, since also GCR increase can be observed along with FD, a term Forbush effect might be more proper (Belov, 2009). The recovery phase of FDs lasts long after the ICME has passed, can frequently be well described as exponential (Lockwood, Webber, and Jokipii, 1986) and can be explained through the global effect of the shock, so called “shadow effect”, where the shock front casts a smaller and smaller “shadow” on the observer as it moves away (for more details see Lockwood, Webber, and Jokipii, 1986; Dumbović *et al.*, 2011). These observations are likely to be related to the global geometry of the interplanetary shock, and not necessarily related to the sheath region that follows.

Based on these considerations, we hypothesize that the shock region should be decoupled from the sheath region when analysing FDs and therefore aim to analyse interaction of GCRs with heliospheric shocks in the context of the FD observations noted above. For that purpose we limit the analysis to high-energy protons (≈ 1 GeV) which typically produce secondary neutrons detected by ground-based neutron monitors. The heliospheric shock structure is quite complex and each of its segments - a foot, a ramp, and an overshoot region (*e.g.* Stone and Tsurutani, 1985) might influence the GCR, however, we will focus on a ramp as the most pronounced feature of the shock. We focus on a single GCR proton, and adopt a test particle approach. We do not adopt a full-orbit particle simulations usually used in particle-in-cell (PIC) models to simulate particle acceleration (*e.g.* Giacalone, 2004) since at 1 AU the collective properties arising from the interaction of the shock at relevant energies (≈ 1 GeV) can be regarded as negligible, as can the particle acceleration at these energies. Acceleration to the GeV energies can occur near the Sun, where the background magnetic field is large, and the intensity of self-excited waves is largest. On the other hand, at 1 AU the background field is much weaker, the wave growth is not as rapid, and the waves are less intense for 1 GeV particles (Desai and Giacalone, 2016). We next assume that the shock structure is laminar and smooth, since any fluctuations can be maximally of the shock size ($\approx 10^4$ km), *i.e.* much smaller than the gyro-radius of our typical particle ($\approx 10^6$ km) and therefore our particle will not see it. We strongly highlight that the assumptions used here are suitable only for the context of highly energetic protons (≈ 1 GeV) interacting with interplanetary shocks typically observed at 1 AU and are therefore not suitable for considerations of *e.g.* solar energetic particles, for which the modelling assumptions and approach should be much different (see *e.g.* Desai and Giacalone, 2016).

It is our intention to analyse GCR-shock interaction depending on key shock characteristics (shock thickness, upstream field strength, B_1 , downstream to upstream field strength ratio, B_2/B_1 , and an inclination angle $\tan \theta = B_{1y}/B_{1x}$) and particle properties (energy, initial speed components) in order to better understand the shock-related Forbush effect. While consequently our analysis might lead to a theoretical model describing the shock-related Forbush effect we note that building such a model would include substantial integration over all incoming directions, for protons of various energies, which is beyond the scope of this paper and will be given elsewhere.

2. Model

Observationally, ICME-related interplanetary shocks resemble fast-mode MHD shocks, since the downstream magnetic field is stronger than the upstream (*e.g.* Kilpua, Koskinen, and Pulkkinen, 2017). Therefore, we consider an oblique 2-dimensional (2D) MHD fast-mode shocks on the GCR protons, where the magnetic field contains components both parallel and normal to the shock front (Figure 1). Regarding the modeling of the high-energy protons behaviour, in such a situation there are several issues that have to be emphasized:

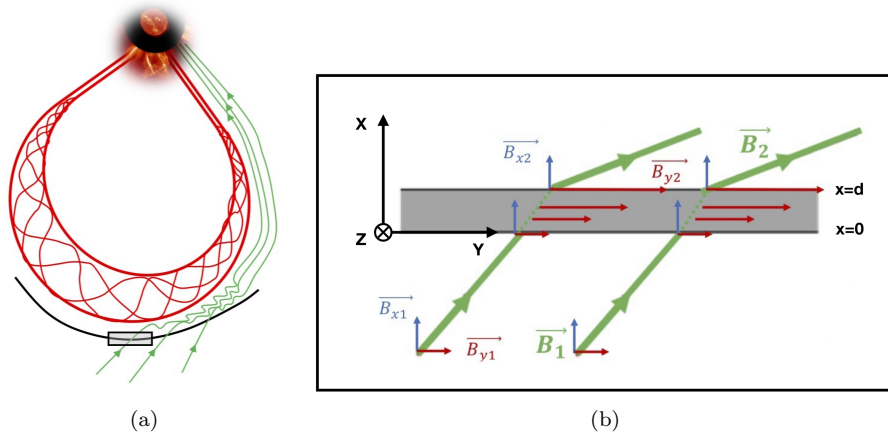


Figure 1. a) Schematic of an interplanetary coronal mass ejection driving a shock ahead of it; b) Enlarged shock region: change of the magnetic field configuration inside an oblique fast-mode MHD shock. Magnetic field in the upstream region ($x < 0$) is weaker than magnetic field in the downstream region ($x > d$).

- Since the shock profile is extremely sharp, *i.e.* its thickness is much smaller than the proton gyro-radius, the “standard” magnetic mirror approximations cannot be applied;
- Due to this, the behaviour of protons turns out to be dependent not only on the upstream/downstream magnetic strength ratio and particle pitch angle, but also on the shock thickness (unlike in the case of the “standard” magnetic mirror approximation);
- We assume an isotropic GCR flux, therefore we allow the test particle to have an arbitrary direction with respect to the shock front;
- The direction of the particle with respect to the shock front does not depend only on the pitch angle, but also on its energy and the impact azimuthal angle ϕ , (see Figure 2) *i.e.*, it depends on the impact direction relative to the magnetic field and the shock surface;
- Consequently, since particle pitch angle alone does not define the direction of the incoming particle with respect to the shock front, for practical reasons, the simplest option for describing the proton behaviour is to follow its trajectory in the Cartesian coordinates defined by the shock characteristic directions.

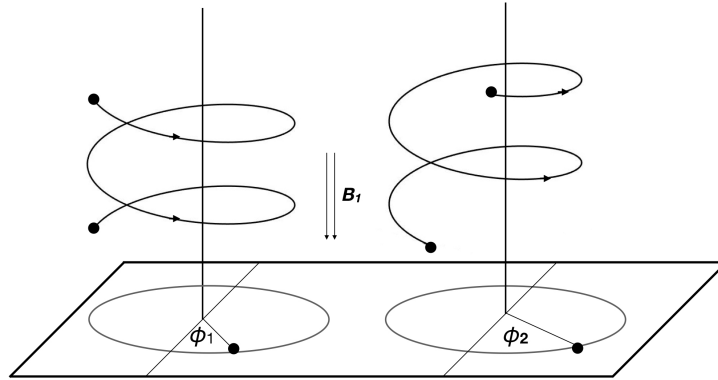


Figure 2. Azimuthal angle ϕ . Particles with different azimuthal angles have different values of speed components at the moment they enter the shock and therefore behave differently inside the shock.

The coordinate system is set so that x -axis is parallel to the shock normal and y -axis is perpendicular to it. According to the magnetic flux conservation the x -component of magnetic field doesn't change. We take the z -component of magnetic field to be zero. The y -component changes from value B_{1y} ahead of the shock (upstream region) to B_{2y} behind the shock (downstream region). Since the magnetic field of fast-mode MHD shock in the downstream region is stronger than magnetic field in the upstream region and the x -component doesn't change, it must be $B_{2y} > B_{1y}$. In our model, we consider the simplest case where the change in y -component of the field across the shock is linear, *i.e.*

$$B_y(x) = B_{1y} + (B_{2y} - B_{1y})\frac{x}{d}, \quad 0 \leq x \leq d. \quad (1)$$

Here $B_y(x)$ is the y -component of the magnetic field inside the shock, d is the shock thickness, and x is the distance from the shock upstream border so that $B_y(0) = B_{1y}$ and $B_y(d) = B_{2y}$.

In the upstream and downstream region the field is homogeneous, so the proton moves in a helical path along the field line. However, the field inside the shock is not homogeneous, so the helical motion of the proton is disrupted (the total speed remains the same since the stationary magnetic field cannot change the proton energy).

The equation of motion

$$\mathbf{F} = m\mathbf{a} = q\mathbf{v} \times \mathbf{B} \quad (2)$$

written in components inside the shock implies:

$$a_x = -\frac{q}{m}v_z B_{1y} - \frac{q}{m}v_z \frac{\Delta B_y}{d}x, \quad (3)$$

$$a_y = \frac{q}{m}v_z B_x, \quad (4)$$

$$a_z = \frac{q}{m}v_x B_{1y} - \frac{q}{m}v_y B_x + \frac{q}{m}v_x \frac{\Delta B_y}{d}x, \quad (5)$$

where $\Delta B_y = B_{2y} - B_{1y}$, and $m = m_0\gamma$ with $\gamma = \sqrt{\frac{1}{1-(\frac{v}{c})^2}}$ the Lorentz factor for a proton with speed v and c is the speed of light.

In the upstream and downstream region components of the equation of motion are respectively

$$a_x = -\frac{q}{m}v_z B_{1y}, \quad (6)$$

$$a_y = \frac{q}{m}v_z B_x, \quad (7)$$

$$a_z = \frac{q}{m}v_x B_{1y} - \frac{q}{m}v_y B_x, \quad (8)$$

and

$$a_x = -\frac{q}{m}v_z B_{2y}, \quad (9)$$

$$a_y = \frac{q}{m}v_z B_x, \quad (10)$$

$$a_z = \frac{q}{m}v_x B_{2y} - \frac{q}{m}v_y B_x. \quad (11)$$

We use the Ordinary Differential Equation (ODE) solver in MATLAB to solve these equations and to obtain proton trajectories for different initial speed components (initial in this context means at the upstream shock border), *i.e.* v_{0x} , v_{0y} and v_{0z} , for protons of different energies and also for shocks with different parameters (shock thickness, upstream field strength, B_1 , downstream to upstream field strength ratio, B_2/B_1 , and an inclination angle $\tan\theta = B_{1y}/B_{1x}$). The used integration method is numerically stable and does not introduce numerical energy gain. However, we note that the numerical energy gain would not affect our results, since this effect happens with each gyration, and in our simulation the gyro-radius is much larger than the shock thickness. The initial conditions correspond to initial speed components. Since a proton of a given energy has a certain total speed, two of its components determine the third. Therefore in the rest of the paper, only proton energy and two speed components will be given and the third one can be easily calculated. We choose to work with v_{0x} and v_{0z} because, for proton to become reflected, v_{0x} needs to decrease and turn negative, and the acceleration in x -direction contains only v_{0z} and not v_{0y} . Trajectories for given shock parameters allow us to see how a certain shock affects protons of different energies, different pitch angles and different incoming directions. In all of the following figures distance in x -direction is scaled to shock thickness d , so the shock thickness is always one, and a distance of for example 10 in x -direction is actually $10d$. Negative values of x represent the upstream region, in particular the distance from the shock border at $x = 0$.

3. Test Proton Examples

As already mentioned, a GCR proton moves in a helical path along the field lines in a homogeneous magnetic field ahead of the shock. After entering the shock, the field is no more homogeneous and the trajectory of the proton starts to change. In this respect we note that the shock thickness is very small compared to the helix radius. Nevertheless, the effect can be quite significant and easily demonstrated (Figure 3) if we look at the proton trajectory before and after the interaction with shock, where “after” doesn’t have to mean “downstream region” because the proton can be reflected back to the upstream region. The simplest case to demonstrate this is that of a longitudinal shock, where the field in the upstream region is parallel to the shock normal, *i.e.* the B_y component is zero. In this case there is no acceleration in the x -direction, and the v_x component of the proton speed doesn’t change in the upstream region (Figure 4). The change starts inside the shock where the proton can be reflected back to upstream region by decreasing the v_x to negative values or transmitted to downstream region (Figure 4). Once the proton is reflected to the upstream region with negative v_x , it continues to move away from the shock without ever coming back. However, since the field lines in the downstream region are not parallel to the shock front, it is possible for a proton to enter the shock region again, due to its helical motion. Then it can be easily accelerated back to the upstream region (Figure 5, blue line). We note that the fact that the proton accelerates in the x -direction does not necessarily imply energy gain, because it decelerates in the y -direction at the same time, and also no electric fields are assumed in these simulations. Alternatively, it is possible for a proton to continue spiral motion in downstream region without ever returning to shock and upstream region (Figure 4, red dashed line). The proton and field parameters in previous examples have no special meaning, they are simply chosen in such a way that resulting figures clearly demonstrate described behaviours. Their values are given in the figure descriptions.

In the general case, for a given field configuration we have similar scenarios. In all of them, a proton is coming from upstream region towards the shock, *i.e.* it has positive x -component of initial speed, $v_{0x} > 0$. Then we have three options:

- i) The x -component of proton speed drops to zero inside the shock and proton is reflected back to the upstream region with $v_x < 0$ where it continues to move away from the shock. In this scenario proton never enters the downstream region.
- ii) A proton that is transmitted to the downstream region does not return to the upstream region but continues its spiral motion in downstream region. These two possibilities are actually the same as in the case of a longitudinal shock.
- iii) The last possibility is somewhat more complicated. A proton can be either reflected to the upstream region or transmitted to the downstream region. Then, due to its helical motion, it can enter the shock region again and repeat this a couple of times (Figure 6). This scenario is of course only possible within

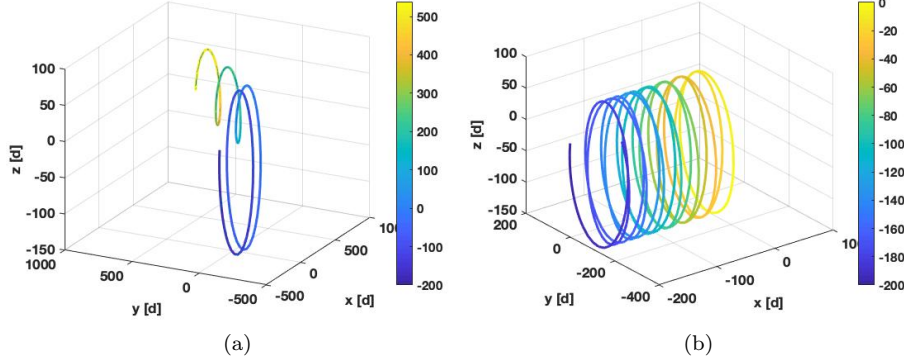


Figure 3. Effect of a longitudinal shock to a 1 GeV proton motion. The initial speed is $v_0 = 0.875c$ and in both cases $v_{0z} = -250\,000\text{ km s}^{-1} = -0.834c$. Shock parameters are: $B_1 = 5\text{ nT}$, $B_2/B_1 = 1.5$, $d = 10\,000\text{ km}$; a) Proton crosses the shock and continues its motion in downstream region with smaller Larmor radius due to the stronger magnetic field. The x -component of the initial speed is: $v_{0x} = 40\,000\text{ km s}^{-1} = 0.133c$ and the pitch angle is $\vartheta = 81.25^\circ$; b) Proton is reflected inside the shock, and returns to the upstream region. The x -component of the initial speed is: $v_{0x} = 10\,000\text{ km s}^{-1} = 0.033c$ and the pitch angle is $\vartheta = 87.84^\circ$.

the Larmor from the shock and since we are only focusing on a near-shock region, we are not interested in the effects occurring in sheath region far away (compared to shock thickness) from the shock.

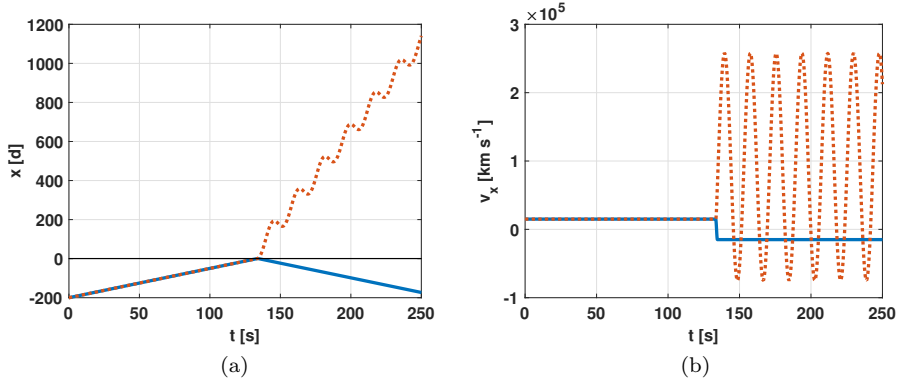


Figure 4. a) Motion in x -direction of two protons with different initial values v_{0z} . Dashed red line represents transmitted proton ($v_{0z} = -250\,000\text{ km s}^{-1} = -0.834c$) and blue solid line a reflected proton ($v_{0z} = 250\,000\text{ km s}^{-1} = 0.834c$). b) Change of v_x component of proton speed for the same two protons. The initial value of v_x is the same in both cases, *i.e.* $v_{0x} = 15\,000\text{ km s}^{-1} = 0.050c$ and therefore the pitch angle is $\vartheta = 86.72^\circ$. Since the shock is a longitudinal shock, the x -component of the speed is a constant in the upstream region. Shock parameters are: $B_1 = 5\text{ nT}$, $B_2/B_1 = 1.5$, $d = 10\,000\text{ km}$.

Whatever the final outcome is, whether the proton ends up in upstream or downstream region, it is important that once the proton is in the downstream

region it can be detected as transmitted. Since some protons will come deeper into the downstream region than others, we will get a smaller number of protons farther away from the shock. So the Forbush decrease amplitude is the smallest near the shock and it is given by the number of particles that never enter the downstream region. The maximum of the amplitude is given by the particles that enter the downstream region, and do not return to the upstream region.

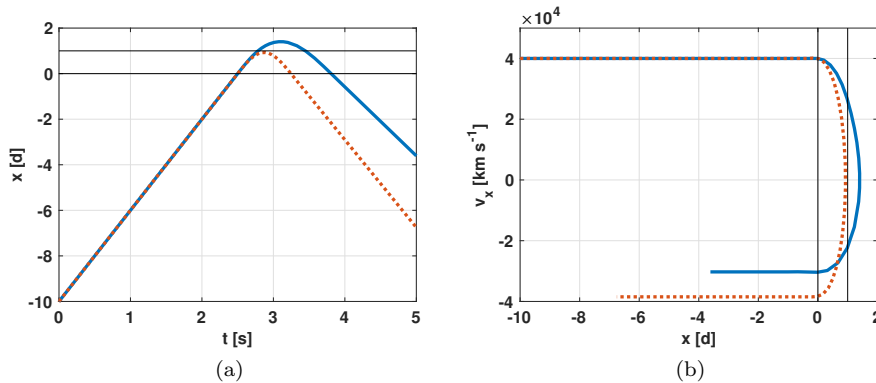


Figure 5. Comparison of a) trajectories and b) x -components of the speed, v_x , for protons reflected inside the longitudinal shock (red dashed line) and behind the same shock in the downstream region (blue solid line). Both protons have the same initial value of v_x , $v_{0x} = 40\,000\text{ km s}^{-1} = 0.133c$ and the pitch angle $\vartheta = 81.25^\circ$, but for the proton reflected inside the shock initial value of v_z is larger *i.e.* $v_{0z} = 259\,000\text{ km s}^{-1} = 0.864c$, and for the proton reflected behind the shock $v_{0z} = 220\,000\text{ km s}^{-1} = 0.734c$. Shock parameters are: $B_1 = 5\text{ nT}$, $B_2/B_1 = 4$, $d = 10\,000\text{ km}$.

4. Analysis of the Parameter Space

Now we examine how a shock with given parameters (shock thickness d , magnetic field in the upstream region B_1 , inclination angle θ and field ratio B_2/B_1) affects proton behavior. We also vary proton energy, *i.e.* proton speed. As our reference point, we take a proton of 1 GeV energy, $B_1 = 5\text{ nT}$ and $B_2/B_1 = 4$ which is the upper limit for perpendicular shock. Typical span of values for shock thickness is between 40 km and 120 000 km (Pinter, 1980). We take for the shock thickness to be $d = 1\,000\text{ km}$ which is approximately the value given in Table 3 in Pinter, (1980). Larger thickness gives particle more time to reflect (*i.e.* more time for v_x to drop to zero) and also results in larger number of reflected particles. This is different from the magnetic mirror case where mirror condition does not depend on the length of trap. However, we have already emphasized that we are not using the magnetic mirror approach because the shock thickness is smaller than the gyro-radius of the proton.

Figure 7 shows the change of v_x component of proton speed inside the shock for different initial conditions. In Figure 7a we vary the initial value of v_x while the initial value of v_z remains the same. For a 1 GeV proton and initial value

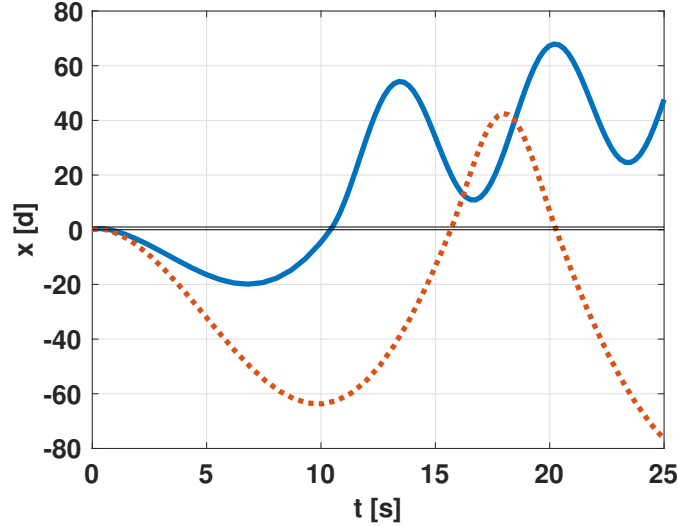


Figure 6. 1 GeV proton trajectories after being reflected inside the shock of strength $B_2/B_1 = 4$, $B_1 = 5$ nT, inclination angle $\theta = 45^\circ$ and thickness $d = 10\,000$ km. Both protons ($v_{0x} = 20\,000$ km s $^{-1} = 0.067c$) are reflected inside the shock back to the upstream region but then enter the shock again. This time they pass the shock and enter the downstream region. One proton continues its motion in downstream region (blue line, $v_{0z} = 150\,000$ km s $^{-1} = 0.500c$, $\vartheta = 50.81^\circ$) and the other is again reflected to the upstream region where it continues its motion (red line, $v_{0z} = 220\,000$ km s $^{-1} = 0.734c$, $\vartheta = 64.20^\circ$).

$v_{0z} = 260\,000$ km s $^{-1} = 0.867c$, v_{0x} has to be smaller than approximately $17\,000$ km s $^{-1} = 0.057c$ (which is more than 10 times smaller than v_{0z}) for the proton to be reflected. On the other hand, if we keep a constant initial value $v_{0x} = 10\,000$ km s $^{-1} = 0.033c$, and vary the initial value of v_z (Figure 7b), we see that the initial value v_{0z} has to be higher than $100\,000$ km s $^{-1} = 0.333c$ for a proton to be reflected. For a proton to be reflected no matter what the initial value v_{0x} was, v_{0z} limiting value should be $261\,918$ km s $^{-1} = 0.874c$, which means 99.80% of total proton speed for 1 GeV proton.

Figure 8 shows that the situation for a longitudinal shock is qualitatively the same, and even quantitatively very similar. The total field is the same as in previous example (5 nT), but the shock inclination angle and therefore field components are different. As it can be seen in graphs, in fields with weaker y -component (*i.e.* longitudinal shocks) v_x will drop to zero for somewhat larger values of v_{0z} . This is in agreement with Equation (3) where stronger B_{1y} results in stronger deceleration a_x . Similar conclusion could be made by “putting” the particle at a perpendicular shock but, since in that case the particle should gyrate parallel to the shock, we omit that analysis here.

In the next step we establish the critical values of v_{0x} and v_{0z} for which the proton is reflected the moment before it would pass the shock (at $x \approx d$). For all the v_{0x} smaller, or v_{0z} larger than those critical values, proton would be reflected inside the shock. This gives us a range of values over which can be integrated to obtain a percentage of protons that are reflected. Since the total proton speed

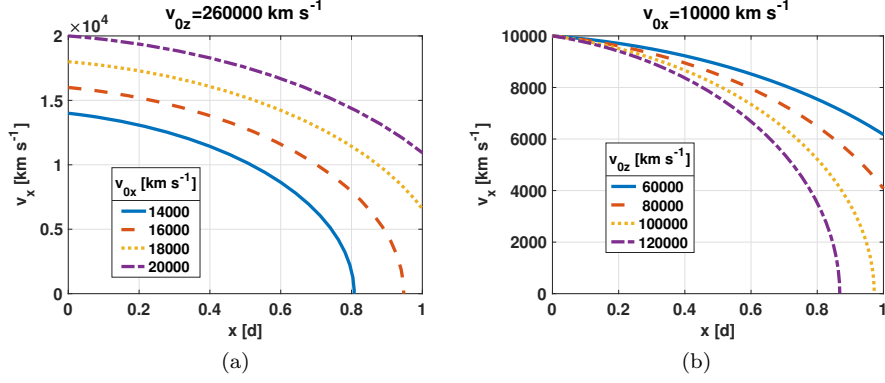


Figure 7. Change of x -component of proton speed inside an oblique shock ($B_1 = 5.0 \text{ nT}$, $B_2/B_1 = 4$ and $\theta = 45^\circ$). Initial conditions are varied for a proton of 1 GeV energy and 1 000 km shock thickness; a) shows the change of v_x with distance from the shock border for different initial values of v_x and constant initial value of v_z , namely $v_{0z} = 260\,000 \text{ km s}^{-1} = 0.867c$; b) shows the change of v_x with distance from the shock for different initial values of v_z and constant initial value of v_x , namely $v_{0x} = 10\,000 \text{ km s}^{-1} = 0.033c$. When v_x becomes zero inside the shock, *i.e.* for $x < 1$, it will continue to decrease and become negative which means that the proton is reflected.

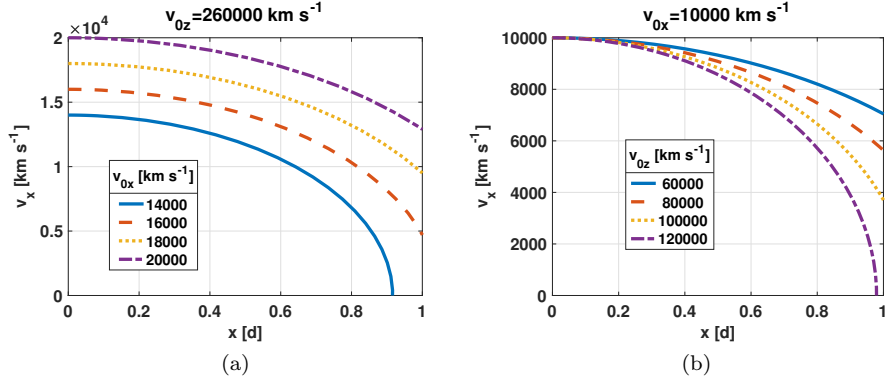


Figure 8. Change of x -component of proton speed inside the longitudinal shock for a proton of 1 GeV energy and 1 000 km shock thickness ($B_1 = 5 \text{ nT}$ and $B_2/B_1 = 4$).

is constant, the value of v_{0y} is determined by chosen v_{0x} and v_{0z} . However, the sign of v_{0z} plays an important role, especially at small v_{0x} and v_{0z} when v_{0y} is large. Negative and large v_{0y} gives large and positive a_z which increases rapidly v_{0z} which in return decreases v_{0x} . This can be seen in Table 1 where for a given v_{0x} , the critical values of v_{0z} are given for positive and negative values of v_{0y} . If v_{0x} is higher than approximately $16\,800 \text{ km s}^{-1} = 0.056c$ the proton will not be reflected no matter what the speed v_{0z} is. For v_{0x} close to this value, critical values of v_{0z} are roughly the same for positive and negative v_{0y} . However, for smaller v_{0x} the critical values of v_{0z} differ greatly for positive and negative v_{0y} .

Table 1. Critical values of v_{0z} for different v_{0x} for positive (second row) and negative (third row) v_{0y} . The values are given in km s^{-1} . Field parameters are $B_1 = 5.0$ nT, $B_2/B_1 = 4$, $\theta = 45^\circ$ and $d = 1\,000$ km.

v_{0x}	1 000	2 000	4 000	8 000	12 000	16 000	16 800
$v_{0z}(v_{0y} > 0)$	19 100	22 400	24 200	63 000	135 400	237 900	261 900
$v_{0z}(v_{0y} < 0)$	0	0	6 900	55 000	130 800	236 000	261 500

Table 2. Critical values of v_{0z} for different v_{0x} and different proton energies. Field parameters are $B_1 = 5.0$ nT, $B_2/B_1 = 4$, $\theta = 45^\circ$ and $d = 1\,000$ km.

E [GeV]	v_{0x} [km s^{-1}]	v_{0z} [km s^{-1}]	v_{0z}/v_0
1	16 800	261 800	0.9974
10	7 550	298 400	0.9983
100	2 490	299 500	0.9983

For 1 GeV protons, $v_{0x} = 16\,800 \text{ km s}^{-1} = 0.056c$ is the maximum value of x -component of initial speed which allows the proton to be reflected. In this case, v_{0z} must be at least $261\,900 \text{ km s}^{-1} = 0.874c$. If we increase proton energy to 10 GeV, we get the maximum value of v_{0x} to be $7\,550 \text{ km s}^{-1} = 0.025c$. For even higher energies of, for example, 100 GeV the maximum value of v_{0x} is even smaller, $2\,480 \text{ km s}^{-1} = 0.008c$. At the same time the initial value of v_{0z} relative to v_0 stays almost the same (Table 2). This indicates that there will be a smaller percentage of reflected particles at higher energies, *i.e.* Forbush decrease will be stronger for lower energy particles in agreement with observational studies showing rigidity dependence of FD magnitude (see *e.g.* Lockwood, 1971; Cane, 2000 and references therein).

Lowering the ratio B_2/B_1 results in a weaker magnetic field behind the shock, B_2 , but also in weaker magnetic field inside the shock which should in turn cause smaller Forbush decrease, qualitatively in agreement with observational studies showing that FD magnitude is larger for larger fields (*e.g.* Belov *et al.*, 2001; Dumbović *et al.*, 2011, 2012; Richardson and Cane, 2011). If we look at the largest possible initial values of v_x (Table 3) we see that they are indeed lower than in previous cases while the corresponding v_{0z} remains almost the same.

Similar effect, but stronger, arises when we decrease the value of the magnetic field in the upstream region, *i.e.* B_1 . If we set $B_1 = 2.5$ nT and $B_2/B_1 = 4$ which results with the same B_2 as in the previous case, we get even smaller maximum values of v_{0x} (see Table 4). In this case the field component B_{1y} is smaller so the x -component of acceleration in Equation (3) is smaller and hence it takes longer time for v_x to become zero.

Finally, Table 5 proves the statement we made at the beginning: for thicker shocks, *i.e.* for larger values of d in Equation (3), larger values of v_{0x} are allowed because even though the deceleration a_x is smaller, there is more time for a particle to get reflected.

Table 3. Critical values of v_{0z} for different v_{0x} and different proton energies. Field parameters are $B_1 = 5.0$ nT, $B_2/B_1 = 2$, $\theta = 45^\circ$ and $d = 1\,000$ km.

E [GeV]	v_{0x} [km s $^{-1}$]	v_{0z} [km s $^{-1}$]	v_{0z}/v_0
1	12 500	261 300	0.9956
10	5 600	298 700	0.9993
100	1 855	299 500	0.9983

Table 4. Critical values of v_{0z} for different v_{0x} and different proton energies. Field parameters are $B_1 = 2.5$ nT, $B_2/B_1 = 4$, $\theta = 45^\circ$ and $d = 1\,000$ km.

E [GeV]	v_{0x} [km s $^{-1}$]	v_{0z} [km s $^{-1}$]	v_{0z}/v_0
1	11 800	261 900	0.9979
10	5 340	298 600	0.9990
100	1 760	299 300	0.9977

5. Conclusion

We presented a model for magnetic field linearly changing inside an oblique 2-dimensional MHD fast-mode shock and used that model to determine whether a proton of certain energy will be reflected inside the shock. We vary initial conditions and solve numerically the set of three differential equations (one for each speed component). The goal is to find such initial conditions that the proton is reflected just at the farther end of the shock. The corresponding initial values of v_x and v_z are called critical values. All v_{0x} smaller than the critical value of v_{0x} and all v_{0z} larger than the critical value of v_{0z} would also result in reflected protons. Obtaining this critical values is an important step in calculating the Forbush decrease amplitude for protons of certain energy. Since we are adjusting initial values, they are only approximate. Their accuracy is within 100 km s^{-1} which is less than 0.04% of the proton speed so the uncertainty is too small to affect the final outcome. Results demonstrate that protons with higher energies are less likely to be reflected. Also, thicker shocks and shocks with larger B_{1y}

Table 5. Critical values of v_{0z} for different v_{0x} and different proton energies. Field parameters are $B_1 = 5.0$ nT, $B_2/B_1 = 4$, $\theta = 45^\circ$ and $d = 10\,000$ km.

E [GeV]	v_{0x} [km s $^{-1}$]	v_{0z} [km s $^{-1}$]	v_{0z}/v_0
1	52 800	256 600	0.9976
10	23 800	296 400	0.9916
100	780	294 000	0.9800

field component reflect more protons than those with smaller. Our next step is to use the obtained results and calculate the Forbush decrease amplitude for different field configurations and particle energies.

Acknowledgments BV and MD acknowledge a support by the Croatian Science Foundation under the project 7549 “Millimeter and submillimeter observations of the solar chromosphere with ALMA”. The research leading to these results has received funding from the European Unions Horizon 2020 research and innovation programme under the Marie Skłodowska-Curie grant agreement No 745782 (ForbMod).

Disclosure of Potential Conflicts of Interest The authors declare that they have no conflicts of interest.

References

- Badruddin, Kumar, A.: 2016, Study of the Cosmic-Ray Modulation During the Passage of ICMEs and CIRs. *Solar Phys.* **291**, 559. DOI. ADS.
- Belov, A.V.: 2009, Forbush effects and their connection with solar, interplanetary and geomagnetic phenomena. In: Gopalswamy, N., Webb, D.F. (eds.) *Universal Heliophysical Processes, IAU Symposium* **257**, 439. DOI. ADS.
- Belov, A.V., Dorman, L.I., Eroshenko, E.A., Iucci, N., Villaresi, G., Yanke, V.G.: 1995, Search for Predictors of Forbush Decreases. In: *International Cosmic Ray Conference, International Cosmic Ray Conference* **4**, 888. ADS.
- Belov, A.V., Eroshenko, E.A., Oleneva, V.A., Struminsky, A.B., Yanke, V.G.: 2001, What determines the magnitude of forbush decreases? *Advances in Space Research* **27**, 625. DOI. ADS.
- Cane, H.V.: 1993, Cosmic ray decreases and magnetic clouds. *J. Geophys. Res.* **98**, 3509. DOI. ADS.
- Cane, H.V.: 2000, Coronal Mass Ejections and Forbush Decreases. *Space Sci. Rev.* **93**, 55. DOI. ADS.
- Cane, H.V., Richardson, I.G., Wibberenz, G.: 1995, The Response of Energetic Particles to the Presence of Ejecta Material. *International Cosmic Ray Conference* **4**, 377. ADS.
- Desai, M., Giacalone, J.: 2016, Large gradual solar energetic particle events. *Living Reviews in Solar Physics* **13**(1), 3. DOI. ADS.
- Dumbović, M., Vršnak, B., Čalogović, J., Karlica, M.: 2011, Cosmic ray modulation by solar wind disturbances. *Astron. Astrophys.* **531**, A91. DOI. ADS.
- Dumbović, M., Vršnak, B., Čalogović, J., Župan, R.: 2012, Cosmic ray modulation by different types of solar wind disturbances. *Astron. Astrophys.* **538**, A28. DOI. ADS.
- Dumbović, M., Heber, B., Vršnak, B., Temmer, M., Kirin, A.: 2018, An Analytical Diffusion-Expansion Model for Forbush Decreases Caused by Flux Ropes. *Astrophys. J.* **860**, 71. DOI. ADS.
- Forbush, S.E.: 1937, On the Effects in Cosmic-Ray Intensity Observed During the Recent Magnetic Storm. *Physical Review* **51**, 1108. DOI. ADS.
- Giacalone, J.: 2004, Large-Scale Hybrid Simulations of Particle Acceleration at a Parallel Shock. *Astrophys. J.* **609**(1), 452. DOI. ADS.
- Hess, V.F., Demmelmair, A.: 1937, World-wide Effect in Cosmic Ray Intensity, as Observed during a Recent Magnetic Storm. *Nature* **140**, 316. DOI. ADS.
- Kilpua, E., Koskinen, H.E.J., Pulkkinen, T.I.: 2017, Coronal mass ejections and their sheath regions in interplanetary space. *Living Reviews in Solar Physics* **14**, 5. DOI. ADS.
- Krymsky, G.F., Krivoshapkin, P.A., Mamrukova, V.P., Gerasimova, S.K.: 2009, Piston shock and Forbush effect. *Astronomy Letters* **35**, 696. DOI. ADS.
- Le Roux, J.A., Potgieter, M.S.: 1991, The simulation of Forbush decreases with time-dependent cosmic-ray modulation models of varying complexity. *Astron. Astrophys.* **243**, 531. ADS.
- Lingri, D., Mavromichalaki, H., Belov, A., Abunina, M., Eroshenko, E., Abunin, A.: 2019, An Extended Study of the Precursory Signs of Forbush Decreases: New Findings over the Years 2008 - 2016. *Solar Phys.* **294**(6), 70. DOI. ADS.

- Lockwood, J.A.: 1971, Forbush decreases in the cosmic radiation. *Space Sci. Rev.* **12**, 658. 10.1007/BF00173346. <http://dx.doi.org/10.1007/BF00173346>.
- Lockwood, J.A., Webber, W.R., Jokipii, J.R.: 1986, Characteristic recovery times of Forbush-type decreases in the cosmic radiation. I - Observations at earth at different energies. *J. Geophys. Res.* **91**, 2851. DOI. ADS.
- Melkumyan, A.A., Belov, A.V., Abunina, M.A., Abunin, A.A., Eroshenko, E.A., Yanke, V.G., Oleneva, V.A.: 2019, Comparison between statistical properties of Forbush decreases caused by solar wind disturbances from coronal mass ejections and coronal holes. *Adv. Space Res.* **63**(2), 1100. DOI. ADS.
- Munakata, K., Yasue, S., Kato, C., Kota, J., Tokumaru, M., Kojima, M., Darwish, A.A., Kuwabara, T., Bieber, J.W.: 2006, On the Cross-Field Diffusion of Galactic Cosmic Rays into an ICME. *Advances in Geosciences, Volume 2: Solar Terrestrial (ST)* **2**, 115. DOI. ADS.
- Papailiou, M., Mavromichalaki, H., Belov, A., Eroshenko, E., Yanke, V.: 2012, Precursor Effects in Different Cases of Forbush Decreases. *Solar Phys.* **276**(1-2), 337. DOI. ADS.
- Parker, E.N.: 1961, Sudden Expansion of the Corona Following a Large Solar Flare and the Attendant Magnetic Field and Cosmic-Ray Effects. *Astrophys. J.* **133**, 1014. DOI. ADS.
- Pinter, S.: 1980, The thickness of interplanetary collisionless shock waves. *Astronomical Institutes of Czechoslovakia* **31**, 368. DOI. ADS.
- Quenby, J.J., Mulligan, T., Blake, J.B., Mazur, J.E., Shaul, D.: 2008, Local and nonlocal geometry of interplanetary coronal mass ejections: Galactic cosmic ray (GCR) short-period variations and magnetic field modeling. *J. Geophys. Res.* **113**, A10102. DOI. ADS.
- Richardson, I.G.: 2004, Energetic Particles and Corotating Interaction Regions in the Solar Wind. *Space Sci. Rev.* **111**, 267. DOI. ADS.
- Richardson, I.G., Cane, H.V.: 2011, Galactic Cosmic Ray Intensity Response to Interplanetary Coronal Mass Ejections/Magnetic Clouds in 1995 - 2009. *Solar Phys.* **270**(2), 609. DOI. ADS.
- Russell, C.T., Mulligan, T.: 2002, On the magnetosheath thicknesses of interplanetary coronal mass ejections. *Planet. Space Sci.* **50**, 527. DOI. ADS.
- Stone, R.G., Tsurutani, B.T.: 1985, Collisionless shocks in the heliosphere: A tutorial review. *Washington DC American Geophysical Union Geophysical Monograph Series* **34**. DOI. ADS.
- Subramanian, P., Antia, H.M., Dugad, S.R., Goswami, U.D., Gupta, S.K., Hayashi, Y., Ito, N., Kawakami, S., Kojima, H., Mohanty, P.K., Nayak, P.K., Nonaka, T., Oshima, A., Sivaprasad, K., Tanaka, H., Tonwar, S.C., The Grapes-3 Collaboration: 2009, Forbush decreases and turbulence levels at coronal mass ejection fronts. *Astron. Astrophys.* **494**, 1107. DOI. ADS.
- Wawrzynczak, A., Alania, M.V.: 2010, Modeling and data analysis of a Forbush decrease. *Advances in Space Research* **45**, 622. DOI. ADS.
- Wibberenz, G., Le Roux, J.A., Potgieter, M.S., Bieber, J.W.: 1998, Transient Effects and Disturbed Conditions. *Space Sci. Rev.* **83**, 309. ADS.